Published in final edited form as:
Biochemistry. 2012 October 30; 51(43): 8597–8607. doi:10.1021/bi3010818.

FTDP-17 tau mutations induce distinct effects on aggregation and microtubule interactions

Benjamin Combs and **T. Chris Gamblin***

Abstract

FTDP-17 mutations in the tau gene lead to early-onset frontotemporal dementias characterized by the pathological aggregation of the microtubule-associated protein tau. Tau aggregation is closely correlated with the progression and severity of localized atrophy of certain regions in the brain. These mutations are primarily located in or near the microtubule-binding repeat regions of tau and can have vastly different effects on the protein. Some mutations have been linked to effects such as increased aggregation, hyperphosphorylation, defects in mRNA splicing, and decreased interaction with microtubules. Given the differential effects of the mutations it may not be surprising that the pathology associated with FTDP-17 can vary widely as well. Despite this variety, several of the mutations are commonly used interchangeably as aggregation inducers for in vitro and in vivo models of tauopathies. We generated recombinant forms of 12 FTDP-17 mutations chosen for their predicted effects on the charge, hydrophobicity, and secondary structure of the protein. We then examined the effects that the mutations had on the properties of in vitro aggregation of the protein and its ability to stabilize microtubule assembly. The group of mutations induced very different effects on the total amount of aggregation, the kinetics of aggregation, and filament morphology. Several of the mutations inhibited the microtubule-stabilization ability of tau while others had very little effect compared to wild-type tau. These results indicate that the mechanisms of disease progression may differ among FTDP-17 mutations and that the effects of the varying mutations may not be equal in all model systems.

Tauopathies are a group of neurodegenerative disorders characterized by the pathological aggregation of the microtubule-associated protein tau. Although tau can be found in a variety of tissues, it is predominantly found in neurons where its primary functions are to promote the assembly and stability of microtubules in addition to interacting with cellular membranes and playing a role in regulation of microtubule spacing as well as axonal transport (1–5). The tau gene contains sixteen exons that, in the central nervous system, give rise to six distinct isoforms that differ by their pattern of inclusion or exclusion of exons 2, 3 and 10. Exon 10 encodes one of four potential microtubule-binding repeat regions (MTBR) that are the primary source of tau interactions with microtubules. Each MTBR contains a

*Corresponding author: Department of Molecular Biosciences, University of Kansas, 1200 Sunnyside Ave., Lawrence, Kansas 66045. Telephone: (785) 864-5065. Fax: (785) 864-5321. gamblin@ku.edu.

Author Contributions

The manuscript was written through contributions of all authors. All authors have given approval to the final version of the manuscript.

SUPPORTING INFORMATION AVAILABLE

Supporting information includes a plot of average filament length and number of filaments for each of the electron micrographs, a graph displaying the correlation between filament length and the ratio of thioflavin S fluorescence to right-angle laser light scattering, and a series of graphs displaying the mean values of all microtubule assembly traces. The information also includes tables of one-way ANOVA analysis with Tukey's Multiple-Comparison test to describe statistical significance of differences in results between pairs of each tau variant in our assays ThS, LLS, tau polymerization kinetics, and microtubule assembly assays. This material is available free of charge via the Internet at http://pubs.acs.org.

highly-conserved 18 amino acid repeat and an inter-repeat regions of 13 or 14 amino acids, both of which make significant contributions microtubule binding (6–8).

Tau MTBR were found to comprise the core of pathologically aggregated tau filaments (9) and have been found to be necessary and sufficient for tau aggregation into straight and paired-helical filaments (10, 11). Within the MTBR, the sequences ^{275}VQIINK in exon 10 and ^{306}VQIVYK in exon 11 misfold into β-strands that subsequently interact with adjacent tau molecules to form characteristic amyloid structure (11–15). The nucleation step, formation of oligomers, is likely the first step in tau aggregation and can be followed by a slower elongation phase that leads to the formation of longer straight or paired helical filaments from these oligomers (16, 17). Aggregated tau then accumulates in pathological structures such as neurofibrillary tangles, neuropil threads, Pick bodies and others that correlate with the type and severity of clinical impairment in neurodegenerative tauopathies (reviewed in (18, 19)).

In Alzheimer's disease and other related tauopathies, tau aggregation is oftentimes associated with other pathological structures such as beta-amyloid extracellular senile plaques. It was therefore unclear whether tau aggregation played a role as a causative agent in neuronal cell death or was simply a byproduct of other toxic mechanisms. The potential for a causative role was greatly strengthened with the identification of a group of mutations in the tau gene that led to early-onset frontotemporal dementias (20, 21). Many of the mutations cause increased propensities for aggregation and decreased microtubule interactions which could represent toxic gain and loss of functions respectively (13, 22–31), Several of the mutations have also been utilized in a diverse set of model organisms, including nematodes, flies, *Xenopus*, and mice ((25, 32–35), reviewed in (36)). These naturally-occurring mutations have provided an invaluable tool to the study of tau aggregation, but their effects have not always been consistent across the spectrum of mutants or model organisms (37).

It is possible that some of the observed differences in the effects of tau aggregation in cellular and animal models are a direct result of the various FTDP-17 mutations employed to generate aggregated tau. Certain FTDP-17 mutations have been shown to increase the rate or total amount of tau aggregation both in vitro and in vivo which may be leading to early-onset tauopathies (22, 26, 34, 38, 39); some FTDP-17 mutants show decreased binding to microtubules and an impaired ability to stabilize polymerization of tubulin while others have little effect (23, 40). In addition, the progression and pathologies of FTDP-17 can vary greatly depending on the specific mutation, indicating that initial causes of the disease may vary as well (reviewed in (41)). We therefore sought to compare several FTDP-17 mutations under the same conditions to determine how they affected aggregation and microtubule interaction, two factors that may have causative roles in the toxicity of these diseases, and whether differences in the intrinsic effects of FTDP-17 mutations could be correlated to these changes. From the 25 known FTDP-17 missense mutants of tau, we chose to model the 12 mutations predicted to have the most significant impact on tau charge, hydrophobicity (42) and structure (43). Our predictions were based on an analysis demonstrating that these parameters were the primary determinants of aggregation rates (44). We chose to model these mutants in the background of full-length 2N4R tau in vitro to provide direct side-by-side comparisons to assess the impact of the structural modifications.

We found that the FTDP-17 mutants had very different effects on the aggregation and microtubule interactions of tau. These changes in aggregate amounts, rates and morphologies could help in our understanding of the varied pathologies and toxicities resulting from the mutations. While some of the mutations had similar effects on tau function and aggregation, we found that there was not a simple correlation between the

effects on tau and the protein's charge, hydrophobicity or predicted structure. This indicates that predictive methods are insufficient for determining the impact of tau mutations on the severity of impairment.

EXPERIMENTAL PROCEDURES

Selection of FTDP-17 mutations

Mutations were selected based on their predicted changes to average hydrophobicity, charge, α-helical structure, β-strand structure, and turns. These predictions were calculated across 7 amino acid-long sequences for the entire 2N4R tau isoform using Kyte-Doolitte values to estimate hydrophobicity (42) and Chou-Fassmann parameters for effects on secondary structure (43). The effect of each mutant was ranked according to each of these factors and the total effect was estimated based on summation of rankings for each variant. The 11 mutants predicted to have the largest effects on the structure of the protein were chosen along with V337M, a mutant commonly used to generate tau aggregation in in vivo models.

Protein expression and purification

All wild-type (WT) and FTDP-17 mutant protein was expressed and purified as described previously (45). The FTDP-17 mutations were created using the Quikchange site-directed mutagenesis kit from Stratagene (La Jolla, CA). The following mutations were generated in a full-length 2N4R tau background contained in a pT7C vector: R5L, G272V, ΔN296, P301L, G303V, L315R, S320F, V337M, E342V, S352L, K369I, and G389R.

Arachidonic acid-induced polymerization

Recombinant WT and mutant tau protein, at a concentration of 2 μM, was incubated in buffer containing 0.1 mM EDTA, 5 mM dithiothreitol, 10 mM Hepes buffer (pH 7.64), 100 mM NaCl, and 3.75% ethanol in a 1.5 mL microcentrifuge tube. The polymerization inducer molecule was arachidonic acid (ARA) at a concentration of 75 μM. Reactions were allowed to proceed overnight at 25 °C.

Thioflavin S fluorescence

The total amount of aggregation was measured utilizing the binding of thioflavin S (ThS) from Sigma-Aldrich (St. Louis, MO). 150 μL of each reaction was added to separate wells in a 96-well, white, flat-bottom plate. ThS was diluted in water and added to the well to a final concentration of 20 μM. The fluorescence shift was measured by using a Cary Eclipse Fluorescence Spectrophotometer (Varian Analytical Instruments, Walnut Valley, CA) with an excitation wavelength of 440 nm and an emission wavelength of 520 nm. PMT voltage was set to 650 V. Readings from a reaction with 2 μM protein and 0 μM ARA were used as a blank and subtracted from the reading for each reaction (45).

Right-angle laser light scattering

Aggregation of the protein was also read by adding 180 μL of the reaction to a 5 mm × 5 mm optical glass fluorometer cuvette (Starna Cells, Atascadero, CA). A 12 mW solid state laser, with a wavelength of λ=532 nm and operating at 7.6 mW, was aimed at the cuvette. The amount of light scattered by particles in the reaction was measured by capturing the amount of light perpendicular to the angle of the beam using a SONY XC-ST270 digital camera. The images were captured at varying aperture settings (from f4 to f11) and analyzed using the histogram function of Adobe Photoshop CS5 version 12.0.1. (25).

ARA-induced polymerization kinetics

ARA was added to our polymerization buffer (0.1 mM EDTA, 5mM dithiothreitol, 10 mM Hepes buffer (pH 7.64), 100 mM NaCl) to a final concentration of 75 μM and 3.75% ethanol in a 5 mm × 5 mm optical glass fluorometer cuvette. Tau polymerization was measured by collecting images of the right-angle scattered light at specific time points beginning from the initiation of the reaction upon addition of protein, at a final concentration of 2 μM, and the ending once the reaction had reached a steady-state. The data were fit to the Finke-Watzky 2-step mechanism, designed to describe the nucleation and elongation of protein aggregation (46). The mechanism assumes simplified nucleation $\left(A \xrightarrow{k_1} B\right)$ and elongation $\left(A+B \xrightarrow{k_2} 2B\right)$ steps to yield the following equation:

$$[B]_t=[A]_0-\frac{\frac{k_1}{k_2}+[A]_0}{1+\frac{k_1}{k_2[A]_0}exp(k_1+k_2[A]_0)t}$$

The k_1 and k_2 rate constants are used to qualitatively compare the rates of nucleation and elongation, respectively, of our protein aggregation reactions.

Transmission electron microscopy

The ARA-induced polymerization reactions were diluted 1:10 in polymerization buffer and 2% glutaraldehyde. After a five minute incubation, a formvar-coated copper grid (Electron Microscopy Sciences, Hatfield, PA) was placed on top of a 10 μL drop of the diluted sample for 1 minute. The grid was then blotted on filter paper, placed on a drop of water, blotted with filter paper, placed on a drop of 2% uranyl acetate, and blotted dry. The grid was then placed on another drop of 2% uranyl acetate for 1 minute and blotted dry for a final time. For all tau variants a single grid was prepared and examined from each of three separate reactions. The grids were examined using a TECNAI G^2 20 electron microscope (FEI Co., Hillsboro, OR). Images were collected with the Gatan Digital Micrograph imaging system at a magnification of 3600X. Five images were collected from each grid and analyzed. The aggregated tau in each of the 15 images was quantified by using Image-Pro Plus 6.0. The macro was designed to recognize filaments with a total perimeter of greater than 30 nm. This captured what we felt to be legitimate aggregates while eliminating background noise. The perimeter of each filament was measured and divided by two in order to estimate the filament's length. These values were totaled in order to estimate the total amount of aggregated material in each image. The total polymerization/image was calculated by taking the mean of all total polymerization values. The mean of all filament lengths was also determined by calculating the mean length of all filaments in a given image and reported as a mean of those values with the error bars representing standard deviation.

Tubulin polymerization assay

The Tubulin Polymerization Assay kit from Cytoskeleton, Inc. (Denver, CO) was used to measure the polymerization of tubulin. The reaction conditions included WT tau or one of the tau variants at 1 μM, or a control compound, added along with 1 mM GTP, 2 mg/ml (~36 μM dimerized) tubulin, 2 mM $MgCl_2$, and 0.5 mM EGTA in 80 mM PIPES buffer at a pH of 6.9. The reaction proceeded in a black, flat-bottomed polystyrene 96-well plate. Paclitaxel was used at 3 μM in one reaction to serve as a positive control for tubulin polymerization, as well as a way to normalize separate reactions. One well contained no additional compound as a negative control. After addition of the compounds the plate was inserted into a FlexStation II Fluorometer (Molecular Devices Corporation, Sunnyvale, CA)

set at a temperature of 37 °C and the reactions were mixed by shaking for 5 seconds. The fluorescence was measured with an excitation wavelength of 355 nm and an emission wavelength at 455 nm at 1 minute intervals for 1 hour. The data were fit to the Gompertz equation

$$y=ae^{-e^{-\frac{t-t_i}{b}}}$$

as described earlier (47, 48). The maximum amount of tubulin polymerization is described by a, the lag time from reaction initiation to the start of polymerization is $t_i - b$, and k_{app}, or $1/b$, is proportional to the rate of polymerization.

Statistical analysis

An unpaired two-tailed Student's t-test was used to compare means of WT values to mean values of each mutant for thioflavin S fluorescence, right-angle laser light scattering, quantitative electron microscopy, and kinetics parameters. A paired two-tailed t-test was used to compare the values for the microtubule assembly assay. P-values less than or equal to 0.05 were indicated with one asterisk (*), less than or equal to 0.01 with two asterisks (**), and less than or equal to 0.001 with three asterisks (***). Because variation among the mutants is also important to consider, statistical variation in the entire groups was measured by using a one-way ANOVA analysis with a Tukey's Multiple Comparison test and compiled in tables included in supplemental information. The p-values for this comparison were also indicated using the asterisk system described above.

RESULTS

Selection of FTDP-17 mutations

A list of 25 known FTDP-17 mutations was generated and ranked based on the total predicted changes to the structure of the protein. The 11 mutations predicted to induce the largest structural changes were selected along with V337M which was selected because it has previously been used in several model organisms. The majority of the chosen FTDP-17 mutations can be found within, or very near to, one of the 4 MTBR while R5L and G389R are found in the N- and C-terminal regions respectively (Figure 1).

FTDP-17 mutations induce varying effects on total polymerization

In vitro experiments were used to examine the effects of the 12 mutations on the ARA-induced polymerization of tau at 2 μM protein and 75 μM ARA (49). After the reactions proceeded overnight, the total amount of aggregation was measured by ThS fluorescence and right-angle laser light scattering (LLS). Half of the mutant proteins displayed an increase in ThS fluorescence compared to WT tau protein (G272V, P301L, G303V, S320F, S352L and G389R), indicating that more protein had polymerized in those reactions. Others had levels of polymerization that were similar to WT tau (R5L, ΔN296, V337M and E342V), while two of the mutants showed a clear decrease (L315R and K369I) (Figure 2A).

LLS can be used as another method to measure relative amounts of protein aggregation (25). However, in this case the results differed from those found in ThS fluorescence. Only three mutants showed a clear increase over WT (R5L, P301L and S352L), while five of the mutants showed a decrease in scattered light (G272V, G303V, L315R, S320F and K369I) and four mutants had levels similar to WT (ΔN296, V337M, E342V and G389R) (Figure 2B). Results from one-way ANOVA analyses with Tukey's multiple comparison tests can be found in Supplemental Tables 1 and 2. This analysis demonstrates that not only are many

of the mutants different from WT, but there is also a wide range in variation between mutants as well.

FTDP-17 mutations induce varying effects on aggregate morphology

Because LLS is known to be affected by the length distribution of the aggregates (25) and the structure of tau recognized by ThS is unknown (16, 50), the aggregates of tau were viewed directly by electron microscopy (Figure 3). Direct visualization of the aggregates can help in elucidating some causes of the apparent variation between the ThS and LLS results (Figure 2). WT tau displays a characteristic mixture of longer filaments and smaller aggregates less than 100 nm in length, hereafter described as oligomers (Figure 3A). Examination of the images made it abundantly clear that the mutations were inducing very different effects on the aggregation of the protein. Some of the mutants, such as G303V and S320F are almost entirely made up of oligomers (Figures 3F and H). Others, including R5L, S352L, and P301L seem to be lacking oligomers and display longer filaments than WT tau (Figures 3B, E, and K). Very few aggregates were associated with K369I which confirms earlier ThS and LLS results (Figures 2 and 3L). We next sought to determine if the apparent differences we observed could be detected by quantitative methods and whether these differences were significant. To accomplish this we measured the number and length of filaments displayed in five representative images from each of three different reactions for each tau variant.

Quantitation of the total amount of aggregated material indicated that most of mutant forms of tau variants polymerized to a similar extent as WT tau but images from G303V, S320F, and E342V all contained more total polymerized tau than WT (Figure 4A). In contrast, K369I and G389R displayed less polymerization than WT in these images. K369I had considerably fewer aggregates than WT and these aggregates were very short in nature and in general did not stain as intensely as tau aggregates associated with WT and the other mutants, again indicating low levels of polymerization (Figures 3L and 4B).

The differences in aggregation, apparent in Figure 3, were confirmed by comparing the average lengths of all filaments for each tau variant. Several mutants (G272V, G303V, L315R, S320F, and G389R) displayed shorter average filament lengths while filaments from R5L, P301L, and S352L were much longer on average than WT (Figure 4B). Average filament lengths are not amenable to statistical analysis due to their exponential distribution. Therefore, the data from each of the 15 electron micrographs were plotted as average filament length versus the number of filaments formed to demonstrate the variation in the data (Supplemental Figure 1). These plots also supported the differences in filament morphology described above. Further variation can be observed by determining how much of the total polymerization is due to very short filaments. We calculated the percent of the total polymerized material that was made up of filaments shorter than 100 nm (Figure 4C). Around 30% of polymerized WT tau was contained in short filaments while oligomers made up greater than 90% of the total for G303V, S320F, and K369I. Others, such as R5L, ΔN296, P301L, and S352L, again induced a very different effect and contained much lower percentages, indicating that longer filament lengths and fewer oligomers were present (Figure 4C).

In light of the quantitative EM data, the discrepancy between ThS fluorescence and LLS measurements of tau mutant aggregation is likely due to the disparate morphologies of the resulting filaments. In fact, there is a direct correlation between filament length, as measured through electron microscopy (Figures 3 and 4B), and the ratio of ThS fluorescence to LLS values (Supplemental Figure 2). Therefore, the amount of light scattering from two populations of filaments of very different length distributions may not be equally proportional to the mass of filaments.

Kinetics of polymerization varies by FTDP-17 mutant

Because the morphology of tau aggregates can be influenced by the rate of polymerization (49), we sought to determine whether the mutations were affecting the kinetics of polymerization. Polymerization reactions for each mutant were followed by LLS and were then fit to a two-step model of polymerization to determine nucleation and elongation rates (Figure 5). The K369I mutant had nearly undetectable levels of polymerization in this assay and could therefore not be fit to the model.

A visual inspection of the curves indicated a wide range of polymerization kinetics between mutants (Figure 5). A comparison of nucleation rates (k1, Figure 6A) indicated that G272V, G303V, L315R, and S320F had significantly increased nucleation rates as compared to WT while R5L, P301L, E342V, and S352L had significantly decreased nucleation rates (Figure 6A). G303V, L315R and S320F also had greatly reduced elongation rates as compared to WT (k2, Figure 6B), such that the elongation phase was essentially undetectable. E342V and S352L had elongation rates that were significantly reduced compared to WT but elongation was still detectable (Figure 6B). The only mutant with a faster elongation rate than WT was P301L (Figure 6B). In addition to these differences from WT protein, further analysis of the data using one-way ANOVA with Tukey's multiple comparison tests demonstrates that many of the mutants are significantly different from one another. For example, the kinetics of elongation (k2) of the P301L mutant is significantly different from G303V, L315R, S320F, V337M, S352L and G389R (Supplemental Tables 3 and 4).

FTDP-17 mutations can inhibit ability of tau to stabilize microtubule assembly or have little effect

We then sought to determine whether the FTDP-17 mutations would have differential effects on one of tau's normal functions of stabilizing microtubules. Microtubule polymerization was monitored using a fluorescence based assay and the resulting curves (Supplemental Figure 3) were fit to a Gompertz function in order to determine maximal extent of microtubule polymerization, the rate of elongation, and lag time in the presence of the FTDP-17 mutants (Figure 7). Most proteins stabilized microtubules to similar levels as WT tau, but G303V, L315R, and S352L did not (Figure 7A). P301L, G303V, S320F, and S352L induced microtubule elongation at a slower rate while V337M and E342V actually increased the rate of tubulin polymerization (Figure 7B). The lag time for tubulin polymerization was decreased in the presence of G272V, L315R, V337M, E342V, and G389R but increased in the presence of G303V and S352L (Figure 7C). In addition to these differences in FTDP-17 mutants as compared to WT, results from one-way ANOVA analyses with Tukey's multiple comparison tests demonstrate that there were many statistically significant differences between FTDP-17 mutants as well (Supplemental Tables 5–7).

DISCUSSION

FTDP-17 mutations in tau are extremely rare but play a particularly important role in the study of tau aggregation associated with familial and sporadic tauopathies. Some of these mutations are commonly used in disease models in order to enhance protein aggregation. However, among the FTDP-17 mutants there exists significant variability in symptoms and pathology of diseases, indicating that there may be differing root causes of the disease. While most known mutations are found within one of the four MTBRs, the locations vary from the N- to the C-terminal regions. The amino acid substitutions or deletions result in increased or decreased hydrophobicity and charge, as well as induce a variety of potential changes in the transient secondary structure of the protein. In addition, other factors such as

alterations in splicing or phosphorylation pattern could be playing a major role in the neurodegenerative process.

Because of the differences in pathology of aggregation and disease progression, it is important to determine how the mutations are changing the properties of the tau protein as well as how these changes could be affecting the associated neurodegeneration patterns. Previous work has shown that the rate of tau aggregation into amyloid could be predicted by calculating expected changes in hydrophobicity, charge, and secondary structure due to three known FTDP-17 mutations (44). In addition, other studies have examined the in vitro properties of small numbers of known mutants (22, 25, 26). We sought to directly compare aggregation and function of WT and a wider variety of FTDP-17 mutant forms of tau under similar conditions, using the same mechanisms for inducing aggregation, as well as to determine whether these predictive tools would apply to an expanded field of mutations.

After studying the effects of FTDP-17 mutations on the in vitro aggregation of tau and its microtubule-stabilization properties we determined that the mutants had very distinct profiles from WT tau as well as each other. We were able to group some of the mutants together based on their common properties and speculate on some of the causes for these general trends although we could not detect a clear pattern between the effects in these assays and the intrinsic changes predicted to occur due to mutations. Some of the mutations induced similar effects on filament morphology that may be tied to their aggregation kinetics, but the overall trends pointed to large differences in the behavior of the mutated versions of tau in our assays.

Several of the mutants displayed shorter average filament lengths than WT which seemed to be due to an increase in the number of oligomers and a decrease in the length and number of longer filaments. The increase in the number of oligomers from this group may be explained by the increased rate of nucleation that was also associated with these four mutations. Fast nucleation would take up large amounts of monomeric tau quickly and drop the protein level below the critical concentration of aggregation before elongation could begin. Interestingly, four of the mutations with decreased filament length occur directly before and after the ^{275}VQIINK and ^{306}VQIVYK sequences, important for aggregation of tau, and may be causing increased nucleation through enhancements of the β-strand character (11, 51). G272V, G303V, and S320F are predicted to enhance β-strand structure and extension of the β-strands in these regions has been shown to enhance polymerization in other mutants, although with slightly different effects (52). The fourth mutation, L315R, is not predicted to enhance β-strand character, but it would replace a hydrophobic amino acid with a positive charge on the polar/charged side of an amphipathic β-strand which may help promote the cross-β amyloid structure (52). Strengthening the β-strand secondary structure in these key regions may increase nucleation; making it more likely that tau will begin to aggregate, leaving little tau left for the elongation phase of polymerization. Therefore the rate of nucleation is an important determinant of the ratio of oligomers to fibrils formed under these conditions.

Another group of mutations induced the opposite effects on the filament morphology phenotype. R5L, P301L, and S352L all induced fewer, but longer filaments, than WT or the other mutant versions of tau. These were slower to nucleate than WT tau which could be another indication of the importance of nucleation rate on filament morphology. Despite the similarities in the rates of nucleation, the elongation rates of these three tau mutants varied widely compared to WT; R5L was similar, P301L was faster, and S352L was slower. Even though each of these mutants aggregated into long filaments with few oligomers, the mechanisms of aggregation were quite dissimilar.

It may seem unusual that R5L, a mutation that is far away from the MTBR, would have such large effects on the aggregation of the protein but the N-terminal region has been shown to have an enhancing effect on aggregation which may be due to alterations in the global hairpin conformation (38, 53, 54). The P301L mutation is much closer to the ^{306}VQIVYK hexapeptide than R5L and the removal of a proline in the PGGG sequence preceding it could assist in the formation of a β-strand in such a way as to stabilize the formation of longer filaments with an altered morphology (55). S352L also enhances the β-strand character around the ^{350}VQLKI sequence which is very similar to the ^{275}VQIINK and ^{306}VQIVYK sequences that form the amphipathic β-strands crucial for the formation of tau filaments. The addition of another amyloidogenic sequence could assist in stabilizing longer filaments.

While the mutants discussed above had obvious effects on the morphology of the aggregates, other mutants, such as ΔN296, V337M, and E342V, displayed aggregates that were much more similar to WT protein. These mutants aggregated into mixes of short and long filaments with roughly the same number of filaments as WT tau. These mutations are further from the ^{275}VQIINK and ^{306}VQIVYK sequences and may not have as strong of effects on those regions even if they are enhancing the β-strand character around them. These minor changes may indicate that the root causes of these tauopathies may lie somewhere other than direct increases in tau aggregation. For example, the N296 position is also associated with other FTDP-17 mutations that can lead to splicing defects and V337M can lead to increased phosphorylation ((31) and reviewed in (56)).

While general trends in the aggregation of mutated proteins could be identified, the interactions with microtubules followed an alternate pattern. Only mutations that occur within one of the 18 amino acid repeats in the MTBR displayed effects on the ability of the protein to stabilize assembly of microtubules, confirming previous results with other FTDP-17 mutations (57). Of the mutants that fell outside of the MTBR or in one of the interrepeats (R5L, L315R, V337M, E342V, K369I, and G389R) only L315R displayed any decrease from WT tau in the total amount of microtubule polymerization. This was a relatively minor change compared to the effects of the other mutants and was in agreement with previous results (58). All of the mutants located within one of the repeat regions were unable to stabilize the same maximum level of microtubule polymerization, stabilized a slower rate of polymerization, or altered the lag time compared to WT tau. These results, combined with the large percentage of FTDP-17 mutations located in a MTBR, indicate that interactions with microtubules may play a key role in the progression of these tauopathies. Further research is needed to determine how altered microtubule interactions may be affecting tau aggregation as well as if affected microtubule dynamics may be playing a more direct role in toxicity.

Direct comparisons of our results to previous studies can be difficult due to differing experimental setup. The most common differences involve the type of tau aggregation inducer employed, the buffer conditions, and the tau isoform used in the assays. Our data confirm previous results indicating that P301L is a very fast aggregator compared to WT, several of these FTDP-17 mutants have decreased abilities to stabilize assembly of microtubules and increased aggregation, and K369I typically forms smaller aggregates (25, 59–61). Occasionally, differences were seen in the kinetics of aggregation that may be ascribed to how the data are measured and what type of curve they are fit to. We feel that the Finke-Watzky mechanism is best able to describe the complex process of tau aggregation in a simplified manner and accurately represented differences in the mechanisms of aggregation for the studied mutations.

The fact that significant differences exist in how these mutants aggregate, the types of aggregates that are seen, as well as their ability to perform normal functions of tau in vitro should not be particularly surprising given the diversity in disease phenotype associated with FTDP-17 cases and tauopathies in general. Conformational differences among the mutations are likely to affect the protein's aggregation in complex ways which could then have a direct impact on disease progression. These differences could manifest themselves in the initiation, morphology, or spread of aggregation. While the end result may always be aggregation of tau and degeneration of neurons, the mechanisms by which the various diseases reach that point may be drastically different and alternate therapeutic interventions may be required based on the initiating cause of the disorder. As it is likely that sporadic tauopathies also differ in their initiating factors, information about how certain FTDP-17 mutations affect tau may be applicable to the progression of those diseases as well.

In order to attempt to explain some of these initiating factors we attempted to find correlations between the intrinsic effects of our chosen mutations and their effects on tau in our various assays. However, we were unable to detect any correlations among these components. It is likely that these effects are complicated and dependent on the specific location of the mutation.

Given the importance of the MTBR in the function and dysfunction of tau, it is likely that location is a very important factor for how these mutations are affecting the aggregation of the protein. Mutations that increased the hydrophobicity and β-strand character, especially in the MTBR, seem to increase the rate of nucleation and decrease the average filament length but exceptions to this exist as well. The causes of familial tauopathies are likely quite complex. Mutation-induced effects on intrinsic properties of tau may alter its propensity for aggregation or the morphology of its aggregates and lead to early-onset tauopathies. However, changes in mRNA splicing, interactions with microtubules, or phosphorylation levels could also lead to aggregation of the protein or neuronal death. In addition, the mutations could also affect other properties of the protein including interactions with protein degradation systems, kinases, or fast axonal transport among others.

Because of the variation in location and effects on intrinsic properties of tau, significant differences exist in how FTDP-17 mutations affect the protein. While these mutations can be quite useful for in vitro and in vivo models of tau aggregation and tauopathies, it may be important to consider the differential effects when comparing results from various model systems. Further work on characterizing these mutations and their effects on in vivo organisms may help explain how the various FTDP-17 mutations are leading to tauopathies and how these mechanisms are affecting our understanding of the progression of sporadic tauopathies.

Supplementary Material

Refer to Web version on PubMed Central for supplementary material.

Acknowledgments

Funding Sources

Support was provided by CurePSP 498-11 (T.C.G.) and NIH GM103418 (T.C.G.)

We thank Akosua Kernizan, James Odum, Yamini Mutreja, Smita Paranjape, Mike Branden, and Sonia Hall for their assistance in generation of the tau mutants and protein purification.

ABBREVIATIONS

ARA	arachidonic acid
FTDP-17	frontotemporal dementia with parkinsonism linked to chromosome 17
LLS	right-angle laser light scattering
MTBR	microtubule-binding repeat region
ThS	thioflavin S
WT	wild-type

References

1. Weingarten MD, Lockwood AH, Hwo SY, Kirschner MW. A protein factor essential for microtubule assembly. Proc Natl Acad Sci U S A. 1975; 72:1858–1862. [PubMed: 1057175]
2. Gauthier-Kemper A, Weissmann C, Golovyashkina N, Sebo-Lemke Z, Drewes G, Gerke V, Heinisch JJ, Brandt R. The frontotemporal dementia mutation R406W blocks tau's interaction with the membrane in an annexin A2-dependent manner. J Cell Biol. 2011; 192:647–661. [PubMed: 21339331]
3. Lee G, Newman ST, Gard DL, Band H, Panchamoorthy G. Tau interacts with src-family non-receptor tyrosine kinases. J Cell Sci. 1998; 111:3167–3177. [PubMed: 9763511]
4. Chen J, Kanai Y, Cowan NJ, Hirokawa N. Projection domains of MAP2 and tau determine spacings between microtubules in dendrites and axons. Nature. 1992; 360:674–677. [PubMed: 1465130]
5. Brandt R, Leger J, Lee G. Interaction of tau with the neural plasma membrane mediated by tau's amino-terminal projection domain. J Cell Biol. 1995; 131:1327–1340. [PubMed: 8522593]
6. Goedert M, Spillantini MG, Potier MC, Ulrich J, Crowther RA. Cloning and sequencing of the cDNA encoding an isoform of microtubule-associated protein tau containing four tandem repeats: differential expression of tau protein mRNAs in human brain. Embo J. 1989; 8:393–399. [PubMed: 2498079]
7. Himmler A, Drechsel D, Kirschner MW, Martin DW Jr. Tau consists of a set of proteins with repeated C-terminal microtubule-binding domains and variable N-terminal domains. Mol Cell Biol. 1989; 9:1381–1388. [PubMed: 2498649]
8. Goode BL, Feinstein SC. Identification of a novel microtubule binding and assembly domain in the developmentally regulated inter-repeat region of tau. J Cell Biol. 1994; 124:769–782. [PubMed: 8120098]
9. Wischik CM, Novak M, Thogersen HC, Edwards PC, Runswick MJ, Jakes R, Walker JE, Milstein C, Roth M, Klug A. Isolation of a fragment of tau derived from the core of the paired helical filament of Alzheimer disease. Proc Natl Acad Sci U S A. 1988; 85:4506–4510. [PubMed: 3132715]
10. Gamblin TC, Berry RW, Binder LI. Modeling tau polymerization in vitro: a review and synthesis. Biochemistry. 2003; 42:15009–15017. [PubMed: 14690409]
11. von Bergen M, Friedhoff P, Biernat J, Heberle J, Mandelkow E. Assembly of tau protein into Alzheimer paired helical filaments depends on a local sequence motif (306VQIVYK311) forming beta structure. Proc Natl Acad Sci U S A. 2000; 97:5129–5134. [PubMed: 10805776]
12. Giannetti AM, Lindwall G, Chau MF, Radeke MJ, Feinstein SC, Kohlstaedt LA. Fibers of tau fragments, but not full length tau, exhibit a cross beta-structure: implications for the formation of paired helical filaments. Protein Sci. 2000; 9:2427–2435. [PubMed: 11206064]
13. Li L, von Bergen M, Mandelkow EM, Mandelkow E. Structure, stability, and aggregation of paired helical filaments from tau protein and FTDP-17 mutants probed by tryptophan scanning mutagenesis. J Biol Chem. 2002; 277:41390–41400. [PubMed: 12198126]
14. Sawaya MR, Sambashivan S, Nelson R, Ivanova MI, Sievers SA, Apostol MI, Thompson MJ, Balbirnie M, Wiltzius JJ, McFarlane HT, Madsen AO, Riekel C, Eisenberg D. Atomic structures of amyloid cross-beta spines reveal varied steric zippers. Nature. 2007; 447:453–457. [PubMed: 17468747]

15. von Bergen M, Barghorn S, Biernat J, Mandelkow EM, Mandelkow E. Tau aggregation is driven by a transition from random coil to beta sheet structure. Biochim Biophys Acta. 2005; 1739:158–166. [PubMed: 15615635]
16. King ME, Ahuja V, Binder LI, Kuret J. Ligand-dependent tau filament formation: implications for Alzheimer's disease progression. Biochemistry. 1999; 38:14851–14859. [PubMed: 10555967]
17. Congdon EE, Kim S, Bonchak J, Songrug T, Matzavinos A, Kuret J. Nucleation-dependent tau filament formation: the importance of dimerization and an estimation of elementary rate constants. J Biol Chem. 2008; 283:13806–13816. [PubMed: 18359772]
18. Lee VM, Goedert M, Trojanowski JQ. Neurodegenerative tauopathies. Annu Rev Neurosci. 2001; 24:1121–1159. [PubMed: 11520930]
19. Sergeant N, Delacourte A, Buee L. Tau protein as a differential biomarker of tauopathies. Biochim Biophys Acta. 2005; 1739:179–197. [PubMed: 15615637]
20. Hutton M, Lendon CL, Rizzu P, Baker M, Froelich S, Houlden H, Pickering-Brown S, Chakraverty S, Isaacs A, Grover A, Hackett J, Adamson J, Lincoln S, Dickson D, Davies P, Petersen RC, Stevens M, de Graaff E, Wauters E, van Baren J, Hillebrand M, Joosse M, Kwon JM, Nowotny P, Heutink P, et al. Association of missense and 5′-splice-site mutations in tau with the inherited dementia FTDP-17. Nature. 1998; 393:702–705. [PubMed: 9641683]
21. Spillantini MG, Murrell JR, Goedert M, Farlow MR, Klug A, Ghetti B. Mutation in the tau gene in familial multiple system tauopathy with presenile dementia. Proc Natl Acad Sci U S A. 1998; 95:7737–7741. [PubMed: 9636220]
22. Arrasate M, Perez M, Armas-Portela R, Avila J. Polymerization of tau peptides into fibrillar structures. The effect of FTDP-17 mutations. FEBS Lett. 1999; 446:199–202. [PubMed: 10100642]
23. Barghorn S, Zheng-Fischhofer Q, Ackmann M, Biernat J, von Bergen M, Mandelkow EM, Mandelkow E. Structure, microtubule interactions, and paired helical filament aggregation by tau mutants of frontotemporal dementias. Biochemistry. 2000; 39:11714–11721. [PubMed: 10995239]
24. DeTure M, Ko LW, Yen S, Nacharaju P, Easson C, Lewis J, van Slegtenhorst M, Hutton M, Yen SH. Missense tau mutations identified in FTDP-17 have a small effect on tau-microtubule interactions. Brain Res. 2000; 853:5–14. [PubMed: 10627302]
25. Gamblin TC, King ME, Dawson H, Vitek MP, Kuret J, Berry RW, Binder LI. In vitro polymerization of tau protein monitored by laser light scattering: method and application to the study of FTDP-17 mutants. Biochemistry. 2000; 39:6136–6144. [PubMed: 10821687]
26. Nacharaju P, Lewis J, Easson C, Yen S, Hackett J, Hutton M, Yen SH. Accelerated filament formation from tau protein with specific FTDP-17 missense mutations. FEBS Lett. 1999; 447:195–199. [PubMed: 10214944]
27. Nagiec EW, Sampson KE, Abraham I. Mutated tau binds less avidly to microtubules than wildtype tau in living cells. J Neurosci Res. 2001; 63:268–275. [PubMed: 11170176]
28. Sahara N, Tomiyama T, Mori H. Missense point mutations of tau to segregate with FTDP-17 exhibit site-specific effects on microtubule structure in COS cells: a novel action of R406W mutation. J Neurosci Res. 2000; 60:380–387. [PubMed: 10797541]
29. Vogelsberg-Ragaglia V, Bruce J, Richter-Landsberg C, Zhang B, Hong M, Trojanowski JQ, Lee VM. Distinct FTDP-17 missense mutations in tau produce tau aggregates and other pathological phenotypes in transfected CHO cells. Mol Biol Cell. 2000; 11:4093–4104. [PubMed: 11102510]
30. Yen SH, Hutton M, DeTure M, Ko LW, Nacharaju P. Fibrillogenesis of tau: insights from tau missense mutations in FTDP-17. Brain Pathol. 1999; 9:695–705. [PubMed: 10517508]
31. Alonso Adel C, Mederlyova A, Novak M, Grundke-Iqbal I, Iqbal K. Promotion of hyperphosphorylation by frontotemporal dementia tau mutations. J Biol Chem. 2004; 279:34873–34881. [PubMed: 15190058]
32. Kraemer BC, Zhang B, Leverenz JB, Thomas JH, Trojanowski JQ, Schellenberg GD. Neurodegeneration and defective neurotransmission in a Caenorhabditis elegans model of tauopathy. Proc Natl Acad Sci U S A. 2003; 100:9980–9985. [PubMed: 12872001]
33. Shulman JM, Feany MB. Genetic modifiers of tauopathy in Drosophila. Genetics. 2003; 165:1233–1242. [PubMed: 14668378]

34. Tanemura K, Akagi T, Murayama M, Kikuchi N, Murayama O, Hashikawa T, Yoshiike Y, Park JM, Matsuda K, Nakao S, Sun X, Sato S, Yamaguchi H, Takashima A. Formation of filamentous tau aggregations in transgenic mice expressing V337M human tau. Neurobiol Dis. 2001; 8:1036–1045. [PubMed: 11741399]
35. Delobel P, Flament S, Hamdane M, Jakes R, Rousseau A, Delacourte A, Vilain JP, Goedert M, Buee L. Functional characterization of FTDP-17 tau gene mutations through their effects on Xenopus oocyte maturation. J Biol Chem. 2002; 277:9199–9205. [PubMed: 11756436]
36. Lee VM, Kenyon TK, Trojanowski JQ. Transgenic animal models of tauopathies. Biochim Biophys Acta. 2005; 1739:251–259. [PubMed: 15615643]
37. Rankin CA, Gamblin TC. Assessing the toxicity of tau aggregation. J Alzheimers Dis. 2008; 14:411–416. [PubMed: 18688091]
38. Gamblin TC, Berry RW, Binder LI. Tau polymerization: role of the amino terminus. Biochemistry. 2003; 42:2252–2257. [PubMed: 12590615]
39. Goedert M, Jakes R. Mutations causing neurodegenerative tauopathies. Biochimica et biophysica acta. 2005; 1739:240–250. [PubMed: 15615642]
40. Hasegawa M, Smith MJ, Goedert M. Tau proteins with FTDP-17 mutations have a reduced ability to promote microtubule assembly. FEBS Lett. 1998; 437:207–210. [PubMed: 9824291]
41. Wszolek ZK, Slowinski J, Golan M, Dickson DW. Frontotemporal dementia and parkinsonism linked to chromosome 17. Folia Neuropathol. 2005; 43:258–270. [PubMed: 16416390]
42. Kyte J, Doolittle RF. A simple method for displaying the hydropathic character of a protein. J Mol Biol. 1982; 157:105–132. [PubMed: 7108955]
43. Chou PY, Fasman GD. Conformational parameters for amino acids in helical, beta-sheet, and random coil regions calculated from proteins. Biochemistry. 1974; 13:211–222. [PubMed: 4358939]
44. Chiti F, Stefani M, Taddei N, Ramponi G, Dobson CM. Rationalization of the effects of mutations on peptide and protein aggregation rates. Nature. 2003; 424:805–808. [PubMed: 12917692]
45. Rankin CA, Sun Q, Gamblin TC. Pseudo-phosphorylation of tau at Ser202 and Thr205 affects tau filament formation. Brain Res Mol Brain Res. 2005
46. Morris AM, Watzky MA, Agar JN, Finke RG. Fitting neurological protein aggregation kinetic data via a 2-step, minimal/"Ockham's razor" model: the Finke-Watzky mechanism of nucleation followed by autocatalytic surface growth. Biochemistry. 2008; 47:2413–2427. [PubMed: 18247636]
47. Sun Q, Gamblin TC. Pseudohyperphosphorylation causing AD-like changes in tau has significant effects on its polymerization. Biochemistry. 2009; 48:6002–6011. [PubMed: 19459590]
48. Combs B, Voss K, Gamblin TC. Pseudohyperphosphorylation has differential effects on polymerization and function of tau isoforms. Biochemistry. 2011; 50:9446–9456. [PubMed: 21942206]
49. Carlson SW, Branden M, Voss K, Sun Q, Rankin CA, Gamblin TC. A complex mechanism for inducer mediated tau polymerization. Biochemistry. 2007; 46:8838–8849. [PubMed: 17608454]
50. Friedhoff P, Schneider A, Mandelkow EM, Mandelkow E. Rapid assembly of Alzheimer-like paired helical filaments from microtubule-associated protein tau monitored by fluorescence in solution. Biochemistry. 1998; 37:10223–10230. [PubMed: 9665729]
51. Li W, Lee VM. Characterization of two VQIXXK motifs for tau fibrillization in vitro. Biochemistry. 2006; 45:15692–15701. [PubMed: 17176091]
52. von Bergen M, Barghorn S, Li L, Marx A, Biernat J, Mandelkow EM, Mandelkow E. Mutations of tau protein in frontotemporal dementia promote aggregation of paired helical filaments by enhancing local beta-structure. J Biol Chem. 2001; 276:48165–48174. [PubMed: 11606569]
53. Jeganathan S, Hascher A, Chinnathambi S, Biernat J, Mandelkow EM, Mandelkow E. Proline-directed pseudo-phosphorylation at AT8 and PHF1 epitopes induces a compaction of the paperclip folding of Tau and generates a pathological (MC-1) conformation. J Biol Chem. 2008; 283:32066–32076. [PubMed: 18725412]
54. Jeganathan S, von Bergen M, Brutlach H, Steinhoff HJ, Mandelkow E. Global hairpin folding of tau in solution. Biochemistry. 2006; 45:2283–2293. [PubMed: 16475817]

55. Mirra SS, Murrell JR, Gearing M, Spillantini MG, Goedert M, Crowther RA, Levey AI, Jones R, Green J, Shoffner JM, Wainer BH, Schmidt ML, Trojanowski JQ, Ghetti B. Tau pathology in a family with dementia and a P301L mutation in tau. J Neuropathol Exp Neurol. 1999; 58:335–345. [PubMed: 10218629]

56. Liu F, Gong CX. Tau exon 10 alternative splicing and tauopathies. Mol Neurodegener. 2008; 3:8. [PubMed: 18616804]

57. LeBoeuf AC, Levy SF, Gaylord M, Bhattacharya A, Singh AK, Jordan MA, Wilson L, Feinstein SC. FTDP-17 mutations in Tau alter the regulation of microtubule dynamics: an “alternative core” model for normal and pathological Tau action. The Journal of biological chemistry. 2008; 283:36406–36415. [PubMed: 18940799]

58. van Herpen E, Rosso SM, Serverijnen LA, Yoshida H, Breedveld G, van de Graaf R, Kamphorst W, Ravid R, Willemsen R, Dooijes D, Majoor-Krakauer D, Kros JM, Crowther RA, Goedert M, Heutink P, van Swieten JC. Variable phenotypic expression and extensive tau pathology in two families with the novel tau mutation L315R. Ann Neurol. 2003; 54:573–581. [PubMed: 14595646]

59. Barghorn S, Zheng-Fischhofer Q, Ackmann M, Biernat J, von Bergen M, Mandelkow E. Structure, microtubule interactions, and paired helical filament aggregation by tau mutants of frontotemporal dementias. Biochemistry. 2000; 39:11714–11721. [PubMed: 10995239]

60. Grover A, DeTure M, Yen SH, Hutton M. Effects on splicing and protein function of three mutations in codon N296 of tau in vitro. Neurosci Lett. 2002; 323:33–36. [PubMed: 11911984]

61. Neumann M, Schulz-Schaeffer W, Crowther RA, Smith MJ, Spillantini MG, Goedert M, Kretzschmar HA. Pick’s disease associated with the novel Tau gene mutation K369I. Ann Neurol. 2001; 50:503–513. [PubMed: 11601501]

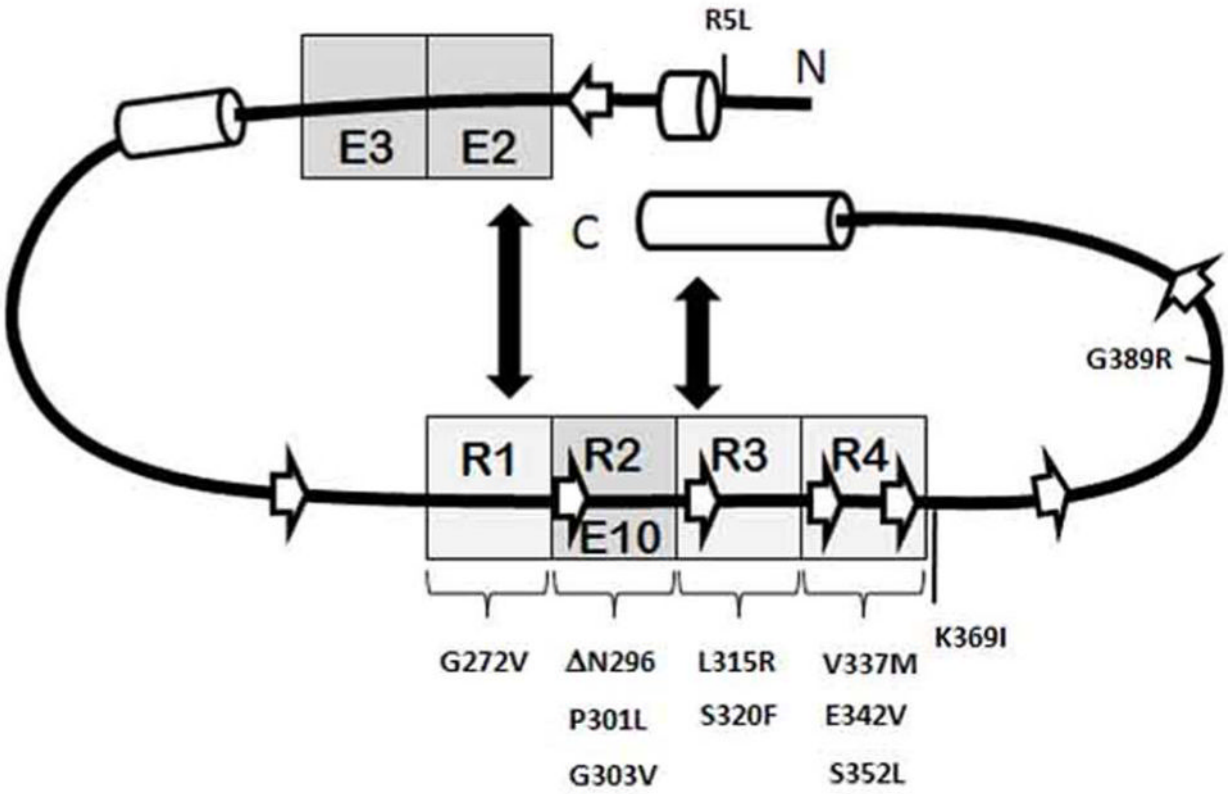

Figure 1. Schematic of FTDP-17 mutations in 2N4R tau

Each of the naturally-occurring FTDP-17 mutations indicated in the figure was created in a full-length 2N4R tau background. E2, E3, and E10 represent exons that can be excluded from other tau isoforms. Regions known to exhibit transient secondary structure are indicated by cylinders (α-helices) or arrows (β-strands). Boxes R1-R4 represent microtubule-binding repeat regions.

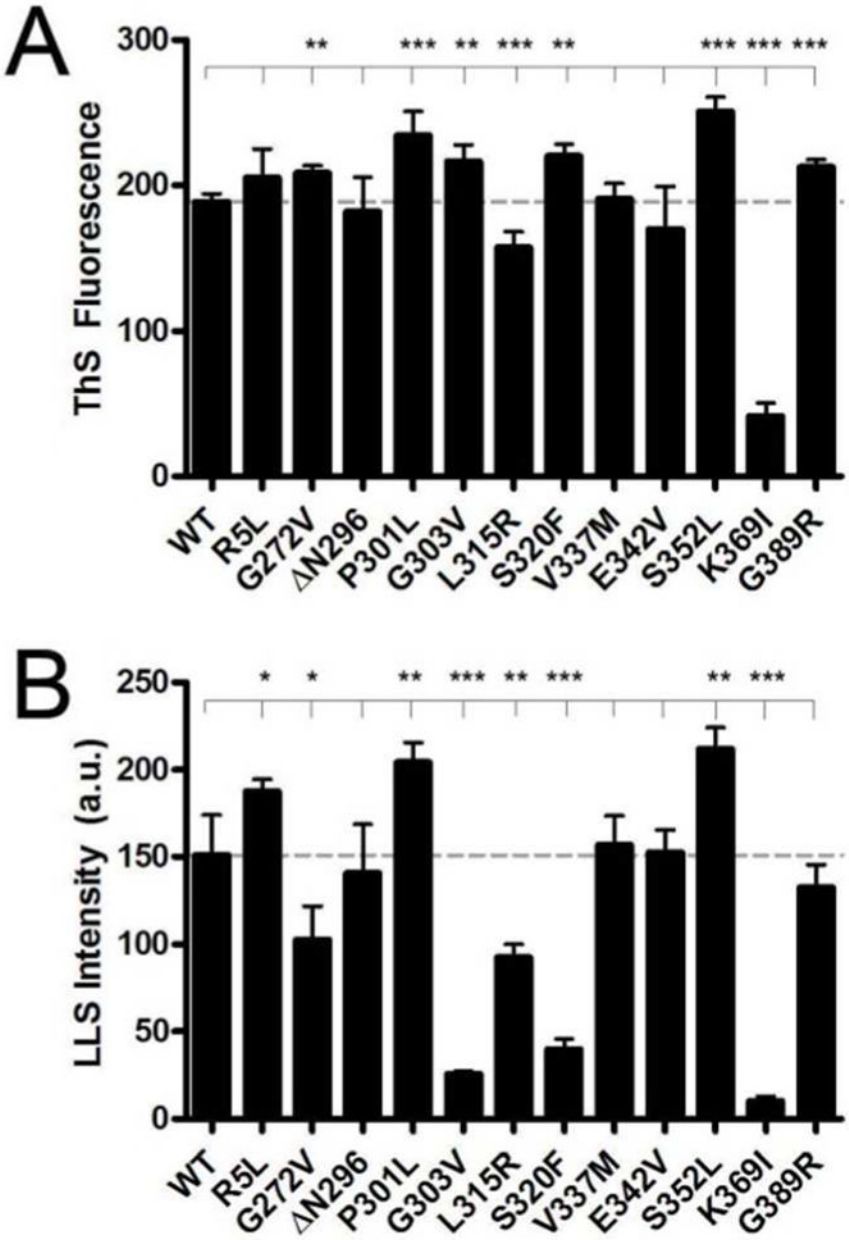

Figure 2. Polymerization of wild-type and FTDP-17 mutant tau measured by thioflavin S staining and right-angle laser light scattering

Polymerization reactions contained 2 μM of WT or one of 12 FTDP-17 mutant versions of tau and 75 μM ARA. Reactions were incubated overnight at 25° C. The final extent of polymerization was measured by (A) ThS fluorescence and (B) right-angle LLS as described in the Experimental Procedures. Data represent the mean from 3 experiments ±SD. Stars represent p-value results from Student's unpaired t tests comparing means from each mutant to WT. (*), $p < 0.05$; (**), $p < 0.01$; (***), $p < 0.001$. More extensive statistical analysis can be found in Supporting Materials.

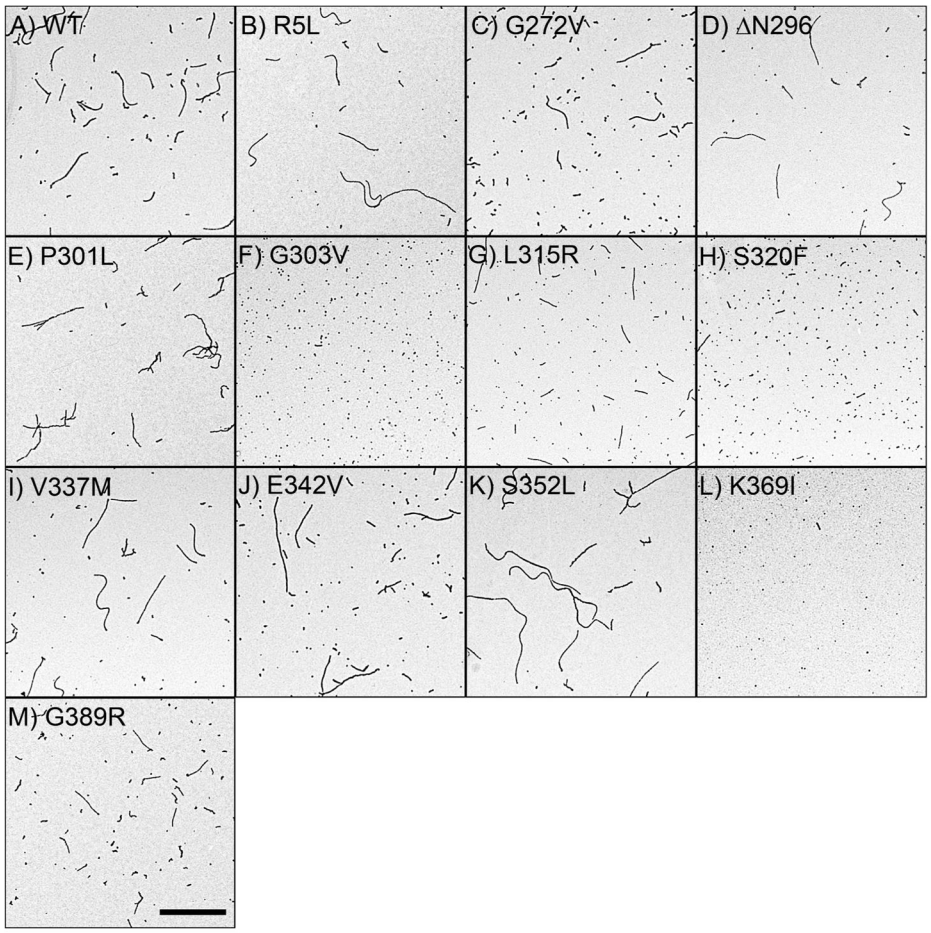

Figure 3. Electron micrographs of polymerization reactions containing 2 μM protein and 75 μM ARA

A representative electron micrograph for (A) WT tau, (B) R5L, (C) G272V, (D) ΔN296, (E) P301L, (F) G303V, (G) L315R, (H) S320F, (I) V337M, (J) E342V, (K) S352L, (L) K369I, and (M) G389R. The scale bar in (M) represents 1 μm and is applicable for all images.

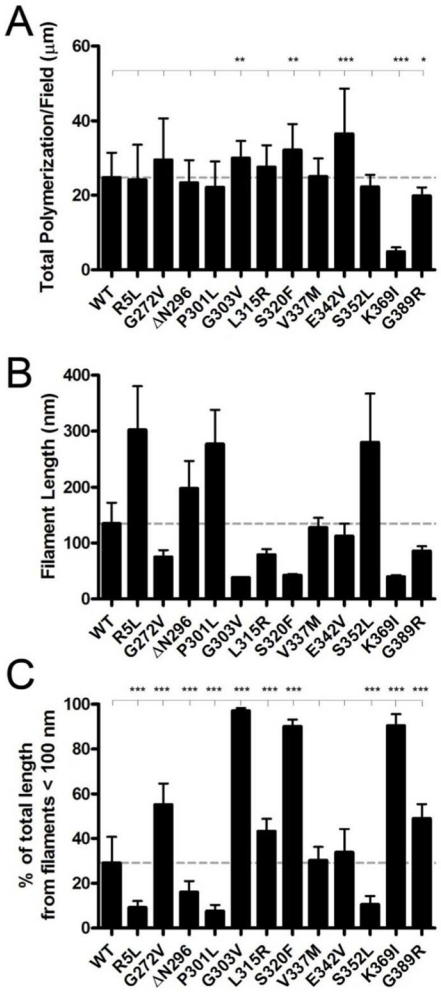

Figure 4. Quantitation of polymerized tau protein in electron micrographs

Images in the electron micrographs from Figure 3 were quantified using Image-Pro Plus 6.0 as described in the Experimental Procedures. The graphs display (A) the mean of the total length (μm) of polymerized tau filaments/image, (B) the mean length of filaments (nm), and (C) the percent of the total length coming from filaments less than 100 nm in length for each of the tau variants. Data in (A) represent the mean of 5 images from each of 3 separate reactions ±SD for a total of n=15. Data in (B) represent the means of the mean filament length for each of the 15 images ±SD. Data in (C) represent means of the sum of all filament lengths less than 100 nm as a percent of the total length for each image ±SD, n=15. Stars represent p-value results from Student's unpaired t tests comparing means from each mutant to WT. (*), $p < 0.05$; (**), $p < 0.01$; (***), $p < 0.001$.

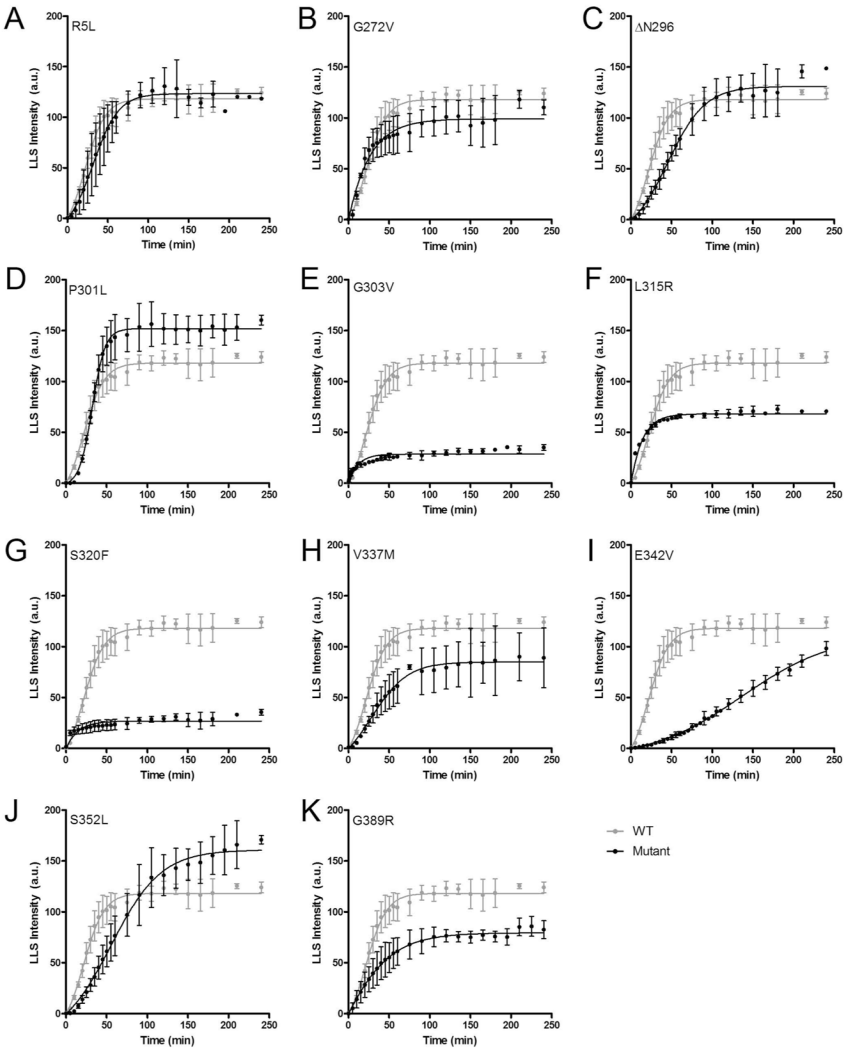

Figure 5. Kinetics of tau polymerization

Polymerization reactions containing 2 μM tau were initiated by the addition of 75 μM ARA. LLS readings were measured at specific time intervals until the reactions reached a steady-state. The traces here represent mean values ±SD from 3 reactions fit to the Finke-Watzky mechanism described in the Experimental Procedures and displayed over 250 minutes for WT tau protein (light gray) and various FTDP-17 mutant tau protein (black) including (A) R5L, (B) G272V, (C) ΔN296, (D) P301L, (E) G303V, (F) L315R, (G) S320F, (H) V337M, (I) E342V, (J) S352L, and (K) G389R.

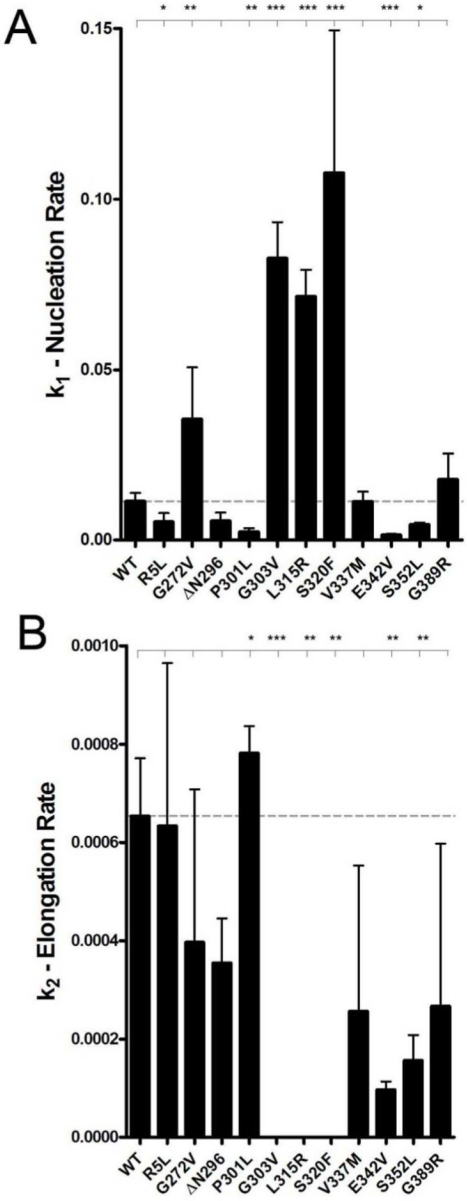

Figure 6. Comparison of tau polymerization kinetics

The parameters describing the tau polymerization kinetics curves fit to the Finke-Watzky mechanism are displayed. The first parameter is (A) k_1, representing the rate of nucleation or formation of oligomers. The second parameter is (B) k_2, the rate of elongation or extension of the oligomeric tau aggregates into filaments. Data represent means of values for fits of at least 3 separate reactions ±SD. Stars represent p-value results from Student's unpaired t tests comparing means from each mutant to WT. (*), $p < 0.05$; (**), $p < 0.01$; (***), $p < 0.001$. More extensive statistical analysis can be found in Supporting Materials.

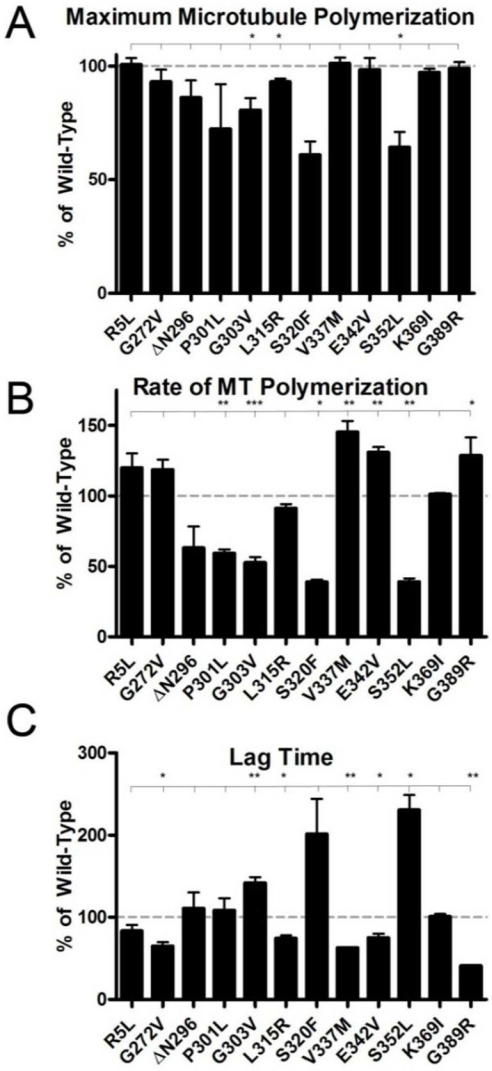

Figure 7. Stabilization of microtubule assembly by tau protein

The tau variants were incubated with tubulin and its polymerization was measured via a fluorescence assay. Numbers were normalized to values of polymerization in the presence of paclitaxel. The relative fluorescence units (*y*-axis) were plotted vs. time (*x*-axis) and fit to the Gompertz equation as described in the Experimental Procedures. From the parameters describing these curves, the percent of WT values for the (A) maximum amount of microtubule polymerization in presence of each protein, (B) k_{app} or rate of microtubule polymerization, and (C) lag time, the time before microtubule polymerization is detected. The values in (A–C) are mean values of the percent changes from WT in three separate experiments ±SD. Stars represent p-value results from Student's paired t tests comparing means from each mutant to WT. (*), $p < 0.05$; (**), $p < 0.01$; (***), $p < 0.001$. More extensive statistical analysis can be found in Supporting Materials.